Many-body effects in the van der Waals–Casimir interaction between graphene layers

Jalal Sarabadani,[1,2] Ali Naji,[3,4,*] Reza Asgari,[4] and Rudolf Podgornik[2,5,6]

[1]*Department of Physics, University of Isfahan, Isfahan 81746, Iran*

[2]*Department of Theoretical Physics, J. Stefan Institute, SI-1000 Ljubljana, Slovenia*

[3]*Department of Applied Mathematics and Theoretical Physics, Centre for Mathematical Sciences, University of Cambridge, Cambridge CB3 0WA, United Kingdom*

[4]*School of Physics, Institute for Research in Fundamental Sciences (IPM), Tehran 19395-5531, Iran*

[5]*Department of Physics, Faculty of Mathematics and Physics, University of Ljubljana, SI-1000 Ljubljana, Slovenia*

[6]*Department of Physics, University of Massachusetts, Amherst, Massachusetts 01003, USA*

(Received 20 May 2011; revised manuscript received 26 August 2011; published 10 October 2011)

Van der Waals-Casimir dispersion interactions between two apposed graphene layers, a graphene layer and a substrate, and in a multilamellar graphene system are analyzed within the framework of the Lifshitz theory. This formulation hinges on a known form of the dielectric response function of an undoped or doped graphene sheet, assumed to be of a random-phase-approximation form. In the geometry of two apposed layers, the separation dependence of the van der Waals-Casimir interaction for both types of graphene sheets is determined and critically compared with some well-known limiting cases. In a multilamellar array, the many-body effects are quantified and shown to increase the magnitude of the van der Waals-Casimir interactions.

DOI: 10.1103/PhysRevB.84.155407 PACS number(s): 03.50.De, 03.70.+k, 05.40.−a, 78.67.−n

I. INTRODUCTION

Graphene appears to be the only known monoatomic two-dimensional (2D) crystal and apart from the intrinsic interest it engenders, it is becoming more and more also a focus of possible and desired advanced technological applications.[1] It is for these reasons that in the past several years we have witnessed a veritable explosion of theoretical and experimental interest in graphene.[2] The Nobel prize for physics in 2010 only consolidated this trend. Graphene differs fundamentally from other known 2D semiconductors because of its unique electronic band structure, viz., the monoatomic sheet of carbon atoms arranged in a honeycomb lattice leads to an electron band structure that displays quite unusual properties.[3] The Fermi surface is reduced to just two points in the Brillouin zone and the value of the band gap is reduced to zero. The energy dispersion relations for both the conduction and the valence bands are linear at low energy, namely, less than 1 eV, meaning that the charge carriers behave as relativistic particles with zero rest mass. The agent responsible for many of the interesting electronic properties of graphene sheets is the non-Bravais honeycomb-lattice arrangement of carbon atoms, which leads to a gapless semiconductor with valence and conduction π bands.

States near the Fermi energy of a graphene sheet are described by a massless Dirac equation that has chiral band states in which the honeycomb-sublattice pseudospin is aligned either parallel or opposite to the envelope function momentum. The Dirac-like wave equation leads to both unusual electron-electron interaction effects and to unusual response to external potentials. When the graphene sheet is chemically doped with either acceptor or donor impurities its carrier mobility can be drastically decreased.[4] Because of its 2D periodic structure, graphene is closely related to single-wall carbon nanotubes, being in fact a carbon nanotube rolled out into a single 2D sheet.[5] The main difference between the electronic properties of single-wall carbon nanotubes and graphene is that the former show circumferential periodicity and curvature that leave their imprint also in the electronic spectrum and consequently also van der Waals (vdW) interactions.[6,7]

On the other hand, graphite appears to be the poor cousin of graphene though it is the stable form of carbon at ordinary temperatures and pressures. Many efforts have been invested into understanding its structural and electronic details (for an account, see Ref. 8). Various known modifications of graphite differ primarily in the way the monoatomic two-dimensional graphene layers stack. Their stacking sequence in terms of commonality is ABA for the Bernal structure, AAA for simple hexagonal graphite or ABC for the rhombohedral graphite.[9]

Graphene layers in graphitic systems are basically closed-shell systems and thus have no covalent bonding between layers, which makes them almost a perfect candidate to study long(er)-ranged nonbonding interactions. Indeed, they are stacked at an equilibrium interlayer spacing of about 0.335 nm and are held together primarily by the nonbonding long-range vdW interactions.[10] Therefore the interaction between graphene layers can be described as a balance between attractive vdW dispersion forces and corrugated repulsive (Pauli) overlap forces,[11] following in this respect closely the paradigm of nanoscale interactions.[12]

Besides a few notable exceptions,[13] until 2009, many electronic and optical properties of graphene could be explained within a single-particle picture in which electron-electron interactions are completely neglected. The discovery of the fractional quantum Hall effect in graphene[14] represents an important hallmark in this context. By now there is a large body of experimental work[15–17] showing the relevance of electron-electron interactions in a number of key properties of graphene samples of sufficiently high quality.

Because of band chirality, the role of electron-electron interactions in graphene sheets differs in some essential ways[18–20] from the role that they play in an ordinary 2D electron gas. One important difference is that the contribution of exchange and correlation to the chemical potential is an increasing rather than a decreasing function of carrier density. This property implies

that exchange and correlation increases the effectiveness of screening, in contrast to the usual case in which exchange and correlation weakens screening.[21] This unusual property follows from the difference in sublattice pseudospin chirality between the Dirac model's negative-energy valence band states and its conduction band states,[18,19] and in a uniform graphene system is readily accounted for by many-body perturbation theory.

In this work, we focus our efforts on the vdW dispersion component of the graphene stacking interaction. Dispersion forces can be formulated on various levels[22] giving mostly consistent results for their strength and separation dependence. In the context of graphene stacking interactions, the problem can be decomposed into the calculation of the dielectric response of the carbon sheets and the subsequent calculation of the vdW interactions either via the quantum-field-theory-based Lifshitz approach, as advocated in this paper, by means of the electron correlation energy[25] or the nonlocal vdW density functional theory.[26] One can show straightforwardly that in fact the nonlocal van der Waals functional approach of the density functional theory and the Lifshitz formalism are in general equivalent.[27]

Specifically, we will calculate the vdW-Casimir interaction free energy per unit area between two graphene sheets as a function of the seperation between them, in a system composed of (a) two apposed undoped or doped graphene sheets, (b) an undoped or a doped graphene layer over a semi-infinite substrate, and (c) a multilayer (infinite) array of graphene sheets. In the latter case, we will investigate the many-body nonpairwise additive effects in the effective interaction between two sheets within a multilayer array. We should note that nonpairwise additive effects are ubiquitous in the context of vdW interactions[22] often leading to nontrivial properties of macromolecular interactions. In this case, they will lead to variations in the equilibrium stacking separation as a function of the number of layers in a graphitic configuration. In the calculation of the vdW-Casimir free energy we will employ the dielectric response function of a single graphene layer calculated previously.[18]

The paper is organized as follows. In Sec. II, we discuss the vdW-Casimir interaction between two undoped or doped graphene sheets. In Sec. III, we consider the case of a graphene sheet apposed to a semi-infinite dielectric substrate. In Sec. IV, we investigate the vdW-Casimir interaction in a system composed of many graphene sheets. We then summarize our main conclusions and compare our results with those available in literature in Sec. V.

II. VDW-CASIMIR INTERACTION BETWEEN TWO LAYERS OF GRAPHENE

The geometry of the system composed of two parallel graphene layers with thicknesses a, facing each other in a bilayer arrangement at a separation b, is shown schematically in Fig. 1. In view of later generalizations, we label the left semi-infinite vacuum space as L, graphene sheets as A, the intervening layer as B, and the right semi-infinite vacuum space by R.

In order to calculate the vdW-Casimir dispersion interaction free energy in the planar geometry, we use the approach of

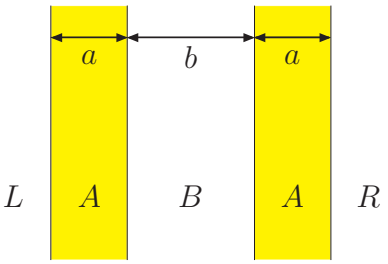

FIG. 1. (Color online) Schematic presentation of two graphene sheets of finite thickness immersed in vacuo at a separation of b. The thickness of both (left and right) layers are equal to a. In view of later generalizations, we have labeled the left semi-infinite vacuum layer with L, the graphene layers with A, the intervening vacuum layer with B, and the right vacuum layer with R. The form of the dielectric functions of the graphene layers is given in Eq. (9).

Ref. 28 where it has been calculated exactly for a multilayer planar geometry. Thus the derived general form of the interaction free energy per unit area includes retardation and thermal effects, being thus valid for any spacing between the layers.

For the system, which is shown schematically in Fig. 1, the vdW-Casimir interaction free energy is obtained in the Lifshitz form as

$$\frac{F_{gg}(b)}{S} = k_B T \sum_{\mathbf{Q}} {\sum_{n=0}^{\infty}}' \ln\left[1 + \frac{\mathcal{D}_1^{(\mathrm{TM})}(\imath\xi_n)}{\mathcal{D}_2^{(\mathrm{TM})}(\imath\xi_n)} e^{-2bk_B(\imath\xi_n)}\right] + [(\mathrm{TM}) \to (\mathrm{TE})], \tag{1}$$

where $F_{gg}(b)$ stands for the graphene-graphene interaction free energy as a function of the layer spacing b (normalized in such a way that it tends to zero at infinite interlayer separation). TM and TE correspond to transverse magnetic and transverse electric modes. In the above Lifshitz formula, the $\mathbf{Q}$ summation is over the transverse wave vector and the n summation (where the prime indicates that the $n = 0$ term has a weight of $1/2$) is over the imaginary Matsubara frequencies

$$\xi_n = \frac{2\pi n k_B T}{\hbar}, \tag{2}$$

where k_B is the Boltzman constant, T is the absolute temperature, and $\hbar$ is the Planck constant divided by 2π. All the quantities in the bracket depend on $\mathbf{Q}$ as well as ξ_n.

The other quantities entering the Lifshitz formula are defined as

$$\begin{aligned}\mathcal{D}_1^{(\mathrm{TM})}(\imath\xi_n) = {} & \Delta_{BA}^{(\mathrm{TM})}(\imath\xi_n)\Delta_{AB}^{(\mathrm{TM})}(\imath\xi_n) \\ & + e^{-2a\kappa_A(\imath\xi_n)}\Delta_{BA}^{(\mathrm{TM})}(\imath\xi_n)\Delta_{RA}^{(\mathrm{TM})}(\imath\xi_n) \\ & + e^{-2a\kappa_A(\imath\xi_n)}\Delta_{AL}^{(\mathrm{TM})}(\imath\xi_n)\Delta_{AB}^{(\mathrm{TM})}(\imath\xi_n) \\ & + e^{-4a\kappa_A}\Delta_{AL}^{(\mathrm{TM})}\Delta_{RA}^{(\mathrm{TM})}, \\ \mathcal{D}_2^{(\mathrm{TM})}(\imath\xi_n) = {} & 1 + e^{-2a\kappa_A(\imath\xi_n)}\Delta_{AB}^{(\mathrm{TM})}(\imath\xi_n)\Delta_{RA}^{(\mathrm{TM})}(\imath\xi_n) \\ & + e^{-2a\kappa_A(\imath\xi_n)}\Delta_{AL}^{(\mathrm{TM})}(\imath\xi_n)\Delta_{AB}^{(\mathrm{TM})}(\imath\xi_n) \\ & + e^{-4a\kappa_A(\imath\xi_n)}\Delta_{AL}^{(\mathrm{TM})}(\imath\xi_n)\Delta_{BA}^{(\mathrm{TM})}(\imath\xi_n) \\ & \times \Delta_{AB}^{(\mathrm{TM})}(\imath\xi_n)\Delta_{RA}^{(\mathrm{TM})}(\imath\xi_n), \end{aligned} \tag{3}$$

with

$$\Delta^{(\mathrm{TM})}_{ii-1}(\imath\xi_n) = \frac{\epsilon_i(\imath\xi_n)\kappa_{i-1}(\imath\xi_n) - \epsilon_{i-1}(\imath\xi_n)\kappa_i(\imath\xi_n)}{\epsilon_i(\imath\xi_n)\kappa_{i-1}(\imath\xi_n) + \epsilon_{i-1}(\imath\xi_n)\kappa_i(\imath\xi_n)}, \quad (4)$$

where $\Delta^{(\mathrm{TM})}_{ii-1}$ quantifies the dielectric discontinuity between homogeneous dielectric layers in the system, where a layer labeled by $i-1$ is located to the left-hand side of the layer labeled by i (for details see Ref. 28). Also $\kappa_i(\imath\xi_n)$ for each electromagnetic field mode within the material i is given by

$$\kappa_i^2(\imath\xi_n) = Q^2 + \frac{\epsilon_i(\imath\xi_n)\mu_i(\imath\xi_n)\xi_n^2}{c^2}, \quad (5)$$

where c is the speed of light in vacuum, Q is the magnitude of the transverse wave vector, and $\epsilon_i(\imath\xi_n)$ and $\mu_i(\imath\xi_n)$ are the dielectric function and the magnetic permeability of the ith layer at imaginary frequencies, respectively. For the sake of simplicity, we assume that for all layers, $\mu_i(\imath\xi_n) = 1$ and that the dielectric function for vacuum layers equals to one for all frequencies.

For the TE modes, everything remains the same except that in this case,

$$\Delta^{(\mathrm{TE})}_{ii-1}(\imath\xi_n) = \frac{\kappa_{i-1}(\imath\xi_n) - \kappa_i(\imath\xi_n)}{\kappa_{i-1}(\imath\xi_n) + \kappa_i(\imath\xi_n)}. \quad (6)$$

The TE part of the vdW free energy is typically much smaller then the TM part and makes a contribution of at most a few percent to the total interaction free energy.

Note that $\epsilon_i(\imath\xi)$ is standardly referred to as the vdW-London dispersion transform of the dielectric function and is defined via the Kramers-Kronig relations as[29]

$$\epsilon(\imath\xi) = 1 + \frac{2}{\pi}\int_0^\infty \frac{\omega\epsilon''(\omega)}{\omega^2+\xi^2}d\omega. \quad (7)$$

It characterizes the magnitude of spontaneous electromagnetic fluctuations at frequency ξ. In general, $\epsilon(\imath\xi)$ is a real, monotonically decaying function of the imaginary argument ξ (for details, see Parsegian's book in Ref. 22).

Lifshitz theory of vdW-Casimir interactions in the form of a Matsubara summation is valid for any material that has a well-defined vdW-London dispersion transform of the frequency dependent dielectric function. This is certainly the case for the random-phase-approximation (RPA) dielectric response that we use in what follows. While for finite thickness layers using a nonlocal dielectric response function in the Lifshitz expression is questionable and requires additional poorly grounded approximations,[23,24] very thin graphene layers yield to the simple approach where one can straightforwardly insert the Q-dependent dielectric function into the Lifshitz formula. For interacting graphene layers of vanishing thickness, this substitution is exact.

In order to proceed, one needs the vdW-London dispersion transform of the dielectric function of all layers in the system. The detailed Q- and ω-dependent forms of the dielectric function for undoped and/or doped graphene layers are introduced in Secs. II A and II B.

A. Two undoped graphene layers

We employ the response function of a graphene layer from Refs. 18 and 30, which for doped graphene assumes the form

$$\chi(Q,\imath\xi_n,\mu\neq 0) = -\frac{g\mu}{2\pi\hbar^2 v^2} - \frac{gQ^2}{16\hbar\sqrt{\xi_n^2+v^2Q^2}} \times\left\{1-\frac{2}{\pi}\mathrm{Re}\left[\arcsin\left(\frac{2\mu+\imath\xi_n\hbar}{vQ\hbar}\right) + \frac{2\mu+\imath\xi_n\hbar}{vQ\hbar}\sqrt{1-\left(\frac{2\mu+\imath\xi_n\hbar}{vQ}\right)^2}\right]\right\}, \quad (8)$$

where $g=4$, $v\approx 10^6$ m/s is the Fermi velocity in graphene layer, and $\mu=\varepsilon_F=\hbar v k_F$ is the chemical potential, ε_F the Fermi energy, and $\hbar k_F$ is the Fermi momentum, where $k_F=(4\pi\rho/g)^{1/2}$ and ρ is the electron density.

To begin with, we assume that two layers are decoupled and ignore the interlayer Coulomb interaction. We comment on this approximation below. The vdW-London dispersion transform of the dielectric function on the level of the RPA is then given by

$$\epsilon(Q,\imath\xi_n) = 1 - V(Q)\chi(Q,\imath\xi_n,\mu\neq 0), \quad (9)$$

where $V(Q)$ is the (transverse) 2D Fourier-Bessel transform of the Coulomb potential, $V(Q)=2\pi e^2/(4\pi\epsilon_0\epsilon_m Q)$, e is the electric charge of electron, ϵ_0 is the permittivity of the vacuum, and ϵ_m is the average of the dielectric constant for the surrounding media, which is equal to one for vacuum. In what follows, we furthermore assume that to the lowest order, the dielectric properties of the graphene layers are not affected by the variation of the separation between them. This assumption is also consistent with the Lifshitz theory that presumes complete independence of the dielectric response functions of the interacting layers.

For undoped graphene layer, i.e., $\rho=0$, the expression for the vdW-London dispersion transform of the dielectric function simplifies substantially and assumes the form

$$\epsilon(Q,\imath\xi_n) = 1 + \frac{\pi\alpha g c Q}{8\epsilon_m v\sqrt{\left(\frac{\xi_n}{v}\right)^2+Q^2}}, \quad (10)$$

where α is the electromagnetic fine-structure constant $\alpha=\frac{e^2}{4\pi\epsilon_0\hbar c}\approx\frac{1}{137}$. It should be noted that, in general, a model going beyond the RPA is necessary in order to account for enhanced correlation effects that would be present in an undoped system.[31] In this paper, however, we restrict ourselves to the RPA approximation and analyze its predictions in detail.

The functional dependence of the interaction free energy of the system per unit area, Eq. (1), is presented in Fig. 2 as a function of the separation between two graphene layers. We assume that the graphene layers are immersed in vacuo and both of them have the same thickness 1 Å as well as equal susceptibilities. Note that in all cases considered in this paper, the interaction free energies as defined in Eq. (1) are negative, reflecting attractive vdW-Casimir force between graphene layers in vacuum. We thus plot the absolute value (magnitude) of the free energy in all cases.

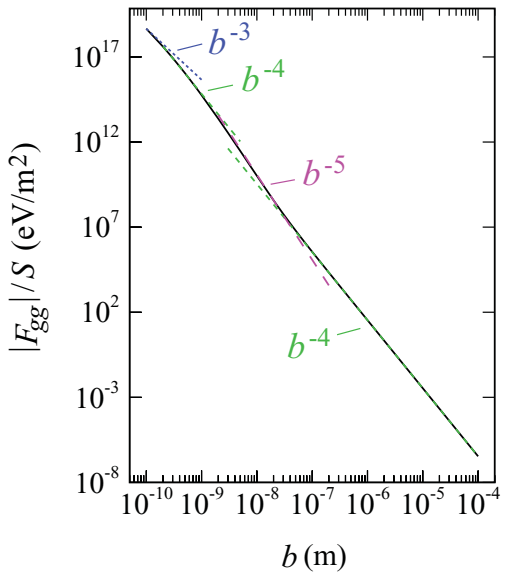

FIG. 2. (Color online) Magnitude of the interaction free energy per unit area of the system composed of two undoped graphene layers immersed in vacuo at an interlayer spacing b and at temperature 300 K. The functional dependence of the interaction free energy on b is compared with the following scaling forms: b^{-3}, b^{-4}, b^{-5}, and b^{-4} as the separation increases.

As one can discern from Fig. 2, the general dependence of the vdW-Casimir interaction free energy on the separation between the graphene layers has the scaling form of a power law b^{-n} with a weakly varying separation-dependent scaling exponent $n(b)$. This scaling exponent can be defined standardly as[22]

$$n(b) = -\frac{d \ln F_{gg}(b)}{d \ln b}. \tag{11}$$

For two undoped graphene sheets, we observe that at small separations, the functional dependence of the free energy on interlayer spacing yields the scaling exponent $n = 3$ for smallest values of the separation. The scaling exponent then steadily increases to $n = 4$, then $n = 5$, and finally, at asymptotically large separations, it reverts back to $n = 4$. This variation in the scaling exponent for the separation dependence of the interaction free energy can be rationalized by invoking some well-known results on the vdW interaction in multilayer geometries (see, e.g., the relevant discussions in Ref. 22).

For example, for two semi-infinite dielectric layers, the interaction free energy should go from the nonretarded form characterized by $n = 2$ for small spacings, through the retarded $n = 3$ form for larger spacings, and then back to zero-frequency-only form for asymptotically large separations that again scales with $n = 2$ but with a different prefactor than the nonretarded form. For two infinitely thin dielectric sheets, on the other hand, we have the nonretarded $n = 4$ form for small separation, followed by the retarded $n = 5$ form for larger spacings, and then reverting back to zero-frequency-only term for asymptotically large separations with $n = 4$ scaling, but again with a different prefactor than the nonretarded limit. Furthermore, the transitions between various scaling forms and the locations of the transition regions are not universal but depend crucially on the characteristics of the dielectric spectra and can thus be quite complicated, sometimes not yielding any easily discernible regimes with a quasiconstant scaling exponent n.

Reading Fig. 2 with this in mind, we can come up with the following interpretation of the calculated separation dependence; for small and vanishing separations, the interaction free energy is dominated by the $n = 3$ form that smoothly approaches the $n = 4$ scaling regime at somewhat larger separations. The $n = 4$ form is consistent with the nonretarded interaction between two very thin dielectric layers, see above, whereas the $n = 3$ scaling is consistent with previous calculations of vdW-Casimir interactions between two graphene sheets at small separation, either at zero or finite temparature.[38,39]

For larger values of the interlayer separations, we then enter the retarded regime with $n = 5$ scaling exponent, again, valid strictly for two infinitely thin layers. This regime of undoped graphene vdW-Casimir interactions has not been identified before. The retarded regime finally gives way to the regime of asymptotically large spacings where the interaction free energy approaches its form given by the zero-frequency term in the Matsubara summation and characterized again by $n = 4$ scaling dependence. Obviously, the numerical coefficient in the small separation nonretarded and asymptotically large separation regimes (both with $n = 4$) are necessarily different.

The interaction free energy scaling with the interlayer separation for two undoped graphene sheets is thus completely consistent with the vdW-Casimir interactions between two thin dielectric layers for all, except for vanishingly small, separations where our calculation gives the same result as previous studies on vdW-Casimir interactions in graphene.[38,39]

The numerical value of the interaction free energy per unit area at 1 nm is about 5.6×10^{14} eV/m^2. That means that for two graphene layers with surface area of 10^{-12} m^2 the magnitude of the free energy is about 560 eV at 1 nm separation; at 10 nm it is about 0.01 eV and at 100 nm about 3.6×10^{-7} eV for the same surface area.

B. Two doped graphene layers

For a doped graphene layer with a finite concentration of mobile charge carriers, the vdW-London dispersion transform of the dielectric function can be read off from Eqs. (9) and (8) as

$$\begin{aligned}
&\epsilon(Q, \imath\xi_n, \mu \neq 0) \\
&\quad = 1 + \frac{2\pi\alpha c}{\epsilon_m Q v}\sqrt{\frac{\rho g}{\pi}} + \frac{\pi\alpha g c Q}{8\epsilon_m v\sqrt{\left(\frac{\xi_n}{v}\right)^2 + Q^2}} \\
&\qquad - \frac{\alpha g c Q}{4\epsilon_m v\sqrt{\left(\frac{\xi_n}{v}\right)^2 + Q^2}}\left\{\arcsin\left[\frac{1}{2}A_1 - \frac{1}{2}B_1\right]\right. \\
&\qquad + 2\sqrt{\frac{4\pi\rho/g}{Q}}\left(A_2^2 + B_2^2\right)^{1/4}\cos\left[\frac{1}{2}\arg(A_2 + \imath B_2)\right] \\
&\qquad \left. - \frac{\xi_n}{vQ}\left(A_2^2 + B_2^2\right)^{1/4}\sin\left[\frac{1}{2}\arg(A_2 + \imath B_2)\right]\right\},
\end{aligned} \tag{12}$$

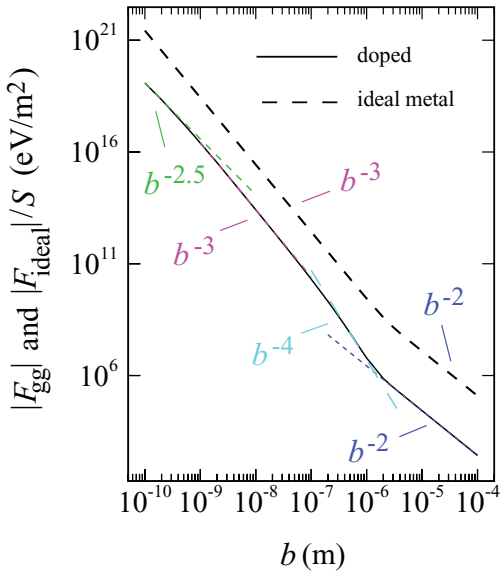

FIG. 3. (Color online) Magnitude of the interaction free energy per unit area of the system composed of two doped graphene layers (solid curve, with the doping electron density $\rho = 10^{16}$ m^{-2}) compared with that of two ideal metallic sheets (dashed curve) immersed in vacuo as a function of the interlayer spacing b, at temperature 300 K. The functional dependence of the free energy on the interlayer spacing is compared with scaling forms $b^{-2.5}$, b^{-3}, b^{-4}, and b^{-2} in various regimes of separation.

with the following coefficients:

$$
\begin{aligned}
A_1 &= \sqrt{\left(\frac{2\sqrt{4\pi\rho/g}}{Q}+1\right)^2+\left(\frac{\xi_n}{vQ}\right)^2},\\
B_1 &= \sqrt{\left(\frac{2\sqrt{4\pi\rho/g}}{Q}-1\right)^2+\left(\frac{\xi_n}{vQ}\right)^2},\\
A_2 &= 1+\left(\frac{\xi_n}{vQ}\right)^2-16\frac{\pi\rho}{gQ^2},\\
B_2 &= -4\frac{\xi_n\sqrt{4\pi\rho/g}}{vQ^2}.
\end{aligned}
\tag{13}
$$

With this dielectric response function we now evaluate the vdW-Casimir interaction free energy of the system per unit area, Eq. (1), as a function of the separation between two graphene layers b as shown in Fig. 3. The interaction free energy has again a scaling form with a scaling exponent varying with the separation between the layers.

As it can be seen from Fig. 3, at vanishingly small separations, the form of the functional dependence of the interaction free energy has $n = 5/2$. Then for increasing spacings, there follows a relatively broad regime with $n = 3$, passing into an $n = 4$ regime, followed eventually by the scaling form with $n = 2$ for $b > 5 \times 10^{-6}$ m.

We can gain some understanding of these regimes by comparing with various previous calculations in the two-layer geometry. For vanishing separations, the $n = 5/2$ regime seen here, has also been observed between thin ideal metallic layers at zero temperature[33,38] or between a graphene sheet on the RPA level and an ideal metallic layer at finite temperatures.[39] Our doped graphene sheet results would thus indicate that the dependence of the vdW-Casimir interactions free energy on the separation could be rationalized in terms of interactions between thin ideal metallic sheets. The $n = 2$ regime for asymptoticaly large separations corresponds to the zero-frequency Matsubara term and has the same scaling form as the finite-temperature vdW-Casimir interaction between two metallic sheets at large separations and has been detected also in the case of a graphene sheet on the RPA level and an ideal metallic layer or between two graphene sheets at finite temperatures.[39] Indeed, it thus seems that the presence of free charges would in fact be a reasonable characterization of doped graphene layers. The regime of intermediate separations corresponds to contributions from progressively higher Matsubara terms leading to $n \simeq 3$–4. It has not been identified before and could present a transition to retardation but also a transition to a more dielectric-like behavior at intermediate separations.

For comparison, we have also plotted the interaction free energy between two ideal metallic sheets, which exhibits a much stronger attractive interaction free energy, i.e.,[22]

$$
\begin{aligned}
\frac{F_{\rm ideal}}{S} &= k_BT\sum_{n=-\infty}^{\infty}\int\frac{d^2p}{(2\pi)^2}\ln[1-e^{-2b\sqrt{p^2+(\xi_n/c)^2}}]\\
&= -\frac{k_BT\zeta(3)}{8\pi b^2}+2k_BT\\
&\quad\times\sum_{n=1}^{\infty}\int\frac{d^2p}{(2\pi)^2}\ln[1-e^{-2b\sqrt{p^2+(\xi_n/c)^2}}].
\end{aligned}
\tag{14}
$$

The numerical value of the energy per unit area at 1 nm is about 2.5×10^{16} eV/m^2, which is equal to 2.5×10^4 eV for surface area of 10^{-12} m^2; at 10 nm, it is about 26 eV and at 100 nm, it is about 0.02 eV for the same surface area.

C. Doped versus undoped graphene

It is instructive to compare the interaction between two graphene layers in the undoped and doped cases. For this purpose, we have plotted the interaction free energy of the system for both cases in Fig. 4. The electron density in doped graphene is assumed to be $\rho = 10^{16}$ m^{-2} (solid curve). The dashed curve is the interaction free energy of the system composed of two undoped graphene layers. As it can be seen, for all separations, the magnitude of the interaction free energy for doped graphene layers is larger than for the undoped case. At separation 1 nm the vdW-Casimir interactions for doped graphene is about 44 times the magnitude of the interaction for undoped graphene, while at the separation of 10 nm this ratio is about 2520. This means that the attractive interaction between graphene layers is enhanced when the contribution of the electron density in the dielectric function of the graphene layers is taken into account. This same trend was observed also in the work of Sernelius[25] and is clearly a consequence of the fact that the largest value of vdW-Casimir interactions is obtained for ideally polarizable, i.e., metallic layers with freely mobile charge carriers. The closer the system is to this idealized case, the larger the corresponding vdW-Casimir interaction will be.

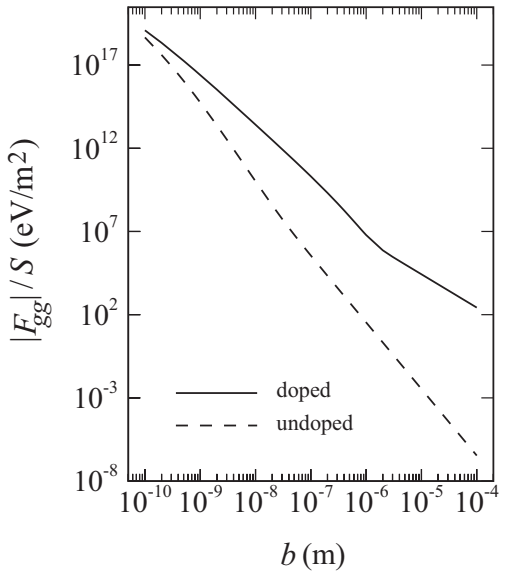

FIG. 4. Magnitude of the free energy per unit area of the system composed of two undoped (dashed line) and doped (solid line) graphene layers (with the electron density $\rho = 10^{16}/\mathrm{m}^2$) immersed in vacuo as a function of the interlayer spacing b, at temperature 300 K. As seen for all separations, the magnitude of the interaction free energy for doped graphene layers is greater than that of the undoped one.

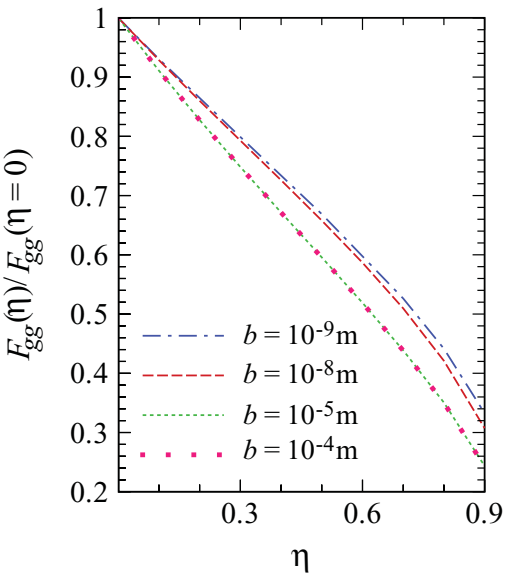

FIG. 5. (Color online) The rescaled interaction free energy $F_{gg}(\eta)/F_{gg}(\eta = 0)$ for the system composed of two doped graphene layers with different electron densities immersed in vacuum as a function of $\eta = (\rho_1 - \rho_2)/(\rho_1 + \rho_2)$ for different interlayer separations $b = 1$ nm, 10 nm, 10 μm, and 100 μm (from top to bottom) at temperature 300 K. Note that $F_{gg}(\eta = 0)$ has been calculated for $\rho_1 = \rho_2 = 10^{16}$ m^{-2}.

Let us investigate also the effect of asymmetry of doped graphene sheets on vdW-Casimir interactions between them. Introducing the dimensionless parameter $\eta = (\rho_1 - \rho_2)/(\rho_1 + \rho_2)$, where ρ_i is the electron density of the ith graphene layer ($i = 1,2$), we find that the interaction free energy depends on the asymmetry in the system. When $\eta = 0$, the electron densities are the same for both graphene layers and we have a symmetric case, whereas $\eta = 1$ means that one of the graphene layers is undoped while the other one is doped, leading to an asymmetric case. In Fig. 5, we have plotted the rescaled free energy $F_{gg}(\eta)/F_{gg}(\eta = 0)$ of the system composed of two graphene layers as a function of η for different values of the interlayer separation. The magnitude of the electron density for one of the layers has been fixed at $\rho_1 = 10^{16}$ m^{-2}, while that of the other layer, ρ_2, varies. As seen from this figure, the curves show a monotonic dependence on η with a stronger interaction at smaller values of η. Note that at large separations, the curves tend to coincide and will become indistinguishable. The asymmetry effects are therefore largest at small separations between the interacting graphene layers.

D. Hamaker coefficient for two graphene layers

The general form of the Hamaker coefficient A_{gg} for a system composed of two dielectric layers of finite thickness (see Fig. 1) when retardation effects are neglected is defined via[22]

$$\frac{F_{gg}(b)}{S} = -\frac{A_{gg}}{12\pi b^2}\left[1 - \frac{2b^2}{(b+a)^2} + \frac{b^2}{(b+2a)^2}\right]. \quad (15)$$

At large separations $b \gg a$, the Hamaker coefficient A_{gg}^{large} can be obtained from

$$\frac{F_{gg}(b)}{S} = -\frac{A_{gg}^{\mathrm{large}} a^2}{2\pi b^4}, \quad (16)$$

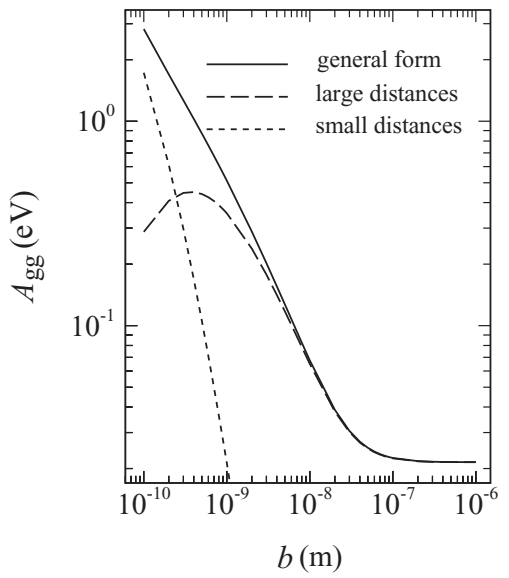

FIG. 6. Hamaker coefficient for a system of two undoped graphene layers as a function of the distance between them b. The top solid line shows the general form of the Hamaker coefficient as defined via Eq. (15), the dashed line shows the limiting large-distance form, Eq. (16), and the dotted line shows the limiting small-distance form, Eq. (17).

while at small separations $b \ll a$, it can be read off from

$$\frac{F_{gg}(b)}{S} = -\frac{A_{gg}^{\text{small}}}{12\pi b^2}. \tag{17}$$

In Fig. 6, we show the Hamaker coefficient as a function of the layer separation for a system of two undoped graphene layers. We show the general form of the Hamaker coefficient from Eq. (15) (solid line) as well as the limiting forms at small [dotted line, Eq. (17)] and large [dashed line, Eq. (16)] separations. The large-distance limiting form obviously coincides with the general form at separations beyond 50 nm. The small-distance limiting form tends to the general form at small separations but given that the thickness of the layers is only about 1 Å, it is expected to merge with the general form in subangstrom separations. For doped graphene, a similar analysis of Eq. (15) is not possible because the corresponding general expression for the interaction free energy is missing.

III. VDW-CASIMIR INTERACTION BETWEEN A GRAPHENE LAYER AND A SEMIINFINITE SUBSTRATE

In this section, we study the interaction between a graphene layer and a semi-infinite dielectric substrate as depicted schematically in Fig. 7. For this system, the free energy per unit area is

$$\frac{F_{sg}(b)}{S} = k_B T \sum_{\mathbf{Q}} {\sum_{n=0}^{\infty}}' \ln\left[1 + \frac{\Delta_{AB}^{(\text{TM})} + \Delta_{RA}^{(\text{TM})} e^{-2a\kappa_A}}{1 + \Delta_{AB}^{(\text{TM})}\Delta_{RA}^{(\text{TM})} e^{-2a\kappa_A}} \times \Delta_{BL}^{(\text{TM})} e^{-2b\kappa_B}\right] + [(\text{TM}) \to (\text{TE})], \tag{18}$$

where F_{sg} now stands for the interaction free energy between the substrate and the graphene layer and we note that for the TE modes, one defines $\Delta_{ij}^{(\text{TE})}$ as in Eq. (6). We have excluded the explicit dependence of the quantities in the bracket on the imaginary Matsubara frequencies, but they are the same as in Eq. (4).

In order to gain insight into the magnitude of the vdW-Casimir interaction free energy and for the sake of simplicity, we assume that the semi-infinite substrate is made of SiO_2,

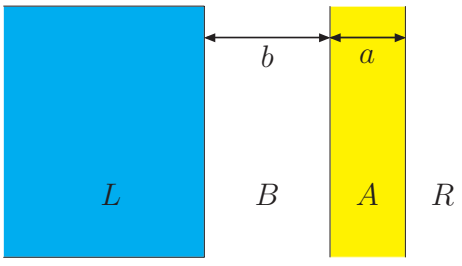

FIG. 7. (Color online) Schematic presentation of a graphene layer of thickness a (labeled by A) apposed to a substrate (labeled by L) at a separation b. We have labeled the intervening layer (assumed to be vacuum) with B, and the right one with R. The dielectric function of the graphene layer is defined via Eq. (9) and for substrate via Eq. (19).

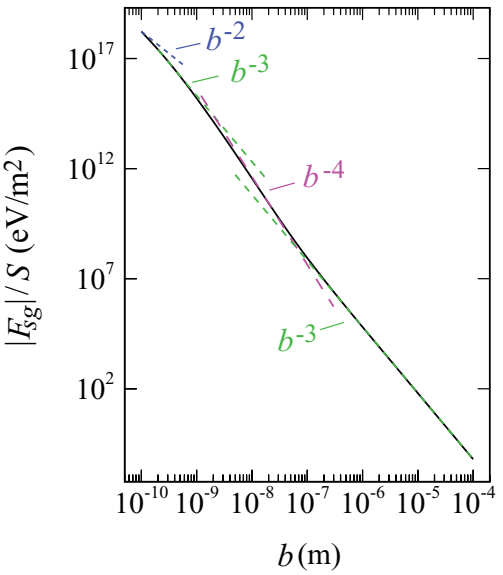

FIG. 8. (Color online) Magnitude of the interaction free energy of the system composed of a SiO_2 substrate and an undoped graphene layer, Eq. (18), plotted at temperature 300 K as a function of the separation b. The functional dependence of the free energy on b is compared with scaling forms b^{-2}, b^{-3}, b^{-4}, and b^{-3} in various regimes of separation.

which has the vdW-London dispersion transform of the dielectric function of the form[22,34]

$$\epsilon_L(\imath\xi_n) = 1 + \frac{C_{\text{UV}}\omega_{\text{UV}}^2}{\xi_n^2 + \omega_{\text{UV}}^2} + \frac{C_{\text{IR}}\omega_{\text{IR}}^2}{\xi_n^2 + \omega_{\text{IR}}^2}, \tag{19}$$

where the values of the parameters, $C_{\text{UV}} = 1.098$, $C_{\text{IR}} = 1.703$, $\omega_{\text{UV}} = 2.033 \times 10^{16}$ rad/s, and $\omega_{\text{IR}} = 1.88 \times 10^{14}$ rad/s, have been determined from a fit to optical data.[35] The static dielectric permittivity of SiO_2 is then obtained as $\epsilon(0) = 3.81$. A characteristic feature of the vdW-London dispersion transform of SiO_2 is thus that it contains two relaxation mechanisms. The first one is due to electronic polarization and the second one is due to ionic polarization. All calculations of the vdW-Casimir interaction free energy are done at room temperature (300 K).

A. Undoped graphene apposed to a substrate

Using the vdW-London dispersion transforms of the dielectric functions given in the preceding sections, one can now calculate the free energy (18) for an undoped graphene layer next to a semi-infinite SiO_2 substrate. The results are shown in Fig. 8.

At vanishingly small separations, the free energy varies with a scaling exponent $n = 2$, while at larger separations one can distinguish the scaling regimes $n = 3$ and $n = 4$, finally approaching the asymptotic zero Matsubara frequency limit at large separations with $n = 3$. This sequence of interaction free energy scalings can be rationalized as follows: at asymptotically large separations, we are at the zero-frequency Matsubara term for a semi-infinite layer and a thin sheet. This case is right in between the asymptotically large separation limit for two semi-infinite layers ($n = 2$) and two infinitely thin layers ($n = 4$). For smaller spacings, we then progressively

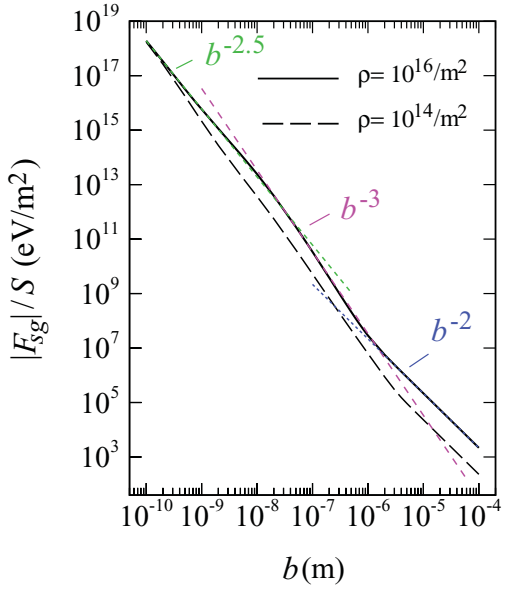

FIG. 9. (Color online) Magnitude of the interaction free energy of the system composed of a SiO_2 substrate and a doped graphene layer, Eq. (18), is plotted at temperature 300 K as a function of the separation b. Here, the functional dependence of the interaction free energy for the graphene doping electron density $\rho = 10^{16}$ m^{-2} (solid line) is compared with scaling forms $b^{-2.5}$, b^{-3}, and b^{-2} in various regimes of separation. We also include the same plot for the doping electron density $\rho = 10^{14}$ m^{-2} (dashed line).

detect contributions from higher Matsubara terms that lead to a scaling exponent $n = 4$ that corresponds to a retarded form of the interaction free energy, and then for yet smaller spacings, the scaling exponent reverts to $n = 3$ nonretarded form of the vdW interaction between a semi-infinite substrate and an infinitely thin sheet. For vanishing spacings, the finite thickness of the sheet starts playing a role and eventually, we approach the $n = 2$ scaling for two semi-infinite layers.

The magnitude of the interaction free energy per unit area at 1 nm is about 1.6×10^{15} eV/m^2. It means that for a system with surface area of 10^{-12} m^2, this value is about 1.6×10^3 eV. At 10 nm, it is about 0.36 eV and at 100 nm, it is about 8.7×10^{-5} eV for the same surface area.

B. Doped graphene apposed to a substrate

The vdW-Casimir interaction free energy (18) for a system composed of a doped graphene layer next to a semi-infinite SiO_2 substrate is shown Fig. 9 for two values of the electron density $\rho = 10^{14}$ m^{-2} (dashed line) and $\rho = 10^{16}$ m^{-2} (solid line).

At vanishingly small separations, the free energy shows the $n = 5/2$ scaling, while for larger spacings, it shows a scaling exponent $n = 3$, approaching the $n \to 2$ limit for asymptotically large separations. The changes in the slope appear to occur at the same values of the interlayer spacing when the electron density decreases (compare dashed and solid curves). Both, the $n = 5/2$ scaling for small separations as well as the $n = 2$ scaling for large separations, suggest, again, that the doped graphene sheet behaves in a similar way as an ideal metallic layer. A related system with a graphene layer apposed to a metallic sheet at finite temperatures has been studied extensively by Gomez-Santos,[39] observing the same scaling exponents as in the case above. One should note, however, that in this work, the model for graphene is closer to what we term doped graphene here.

The magnitude of the free energy for the electron density $\rho = 10^{14}$ m^{-2} (dashed line) and surface area of 10^{-12} m^2 at 1 nm is about 2.1×10^3 eV, while at 10 nm, it is about 3.7 eV, and at 100 nm, is about 5.2×10^{-3} eV.

These values increase for larger electron densities, e.g., for $\rho = 10^{16}$ m^{-2} (solid line) and the same surface area, the free energy magnitude is 5.9×10^3 eV at 1 nm, while it is about 24 eV at 10 nm and about 3.4×10^{-2} eV at 100 nm.

C. Hamaker coefficient for the graphene-substrate system

The general form of the Hamaker coefficient A_{sg} for a system composed of a dielectric layer of finite thickness apposed to a semiinfinite dielectric substrate (see Fig. 7) when retardation effects are neglected is defined via[22]

$$\frac{F_{sg}(b)}{S} = -\frac{A_{sg}}{12\pi b^2}\left[1 - \frac{b^2}{(b+a)^2}\right]. \tag{20}$$

At large separations $b \gg a$, the Hamaker coefficient A_{sg}^{large} can be obtained from

$$\frac{F_{sg}(b)}{S} = -\frac{A_{sg}^{\text{large}} a}{6\pi b^3}, \tag{21}$$

while at small separations $b \ll a$, it can be read off from

$$\frac{F_{sg}(b)}{S} = -\frac{A_{sg}^{\text{small}}}{12\pi b^2}. \tag{22}$$

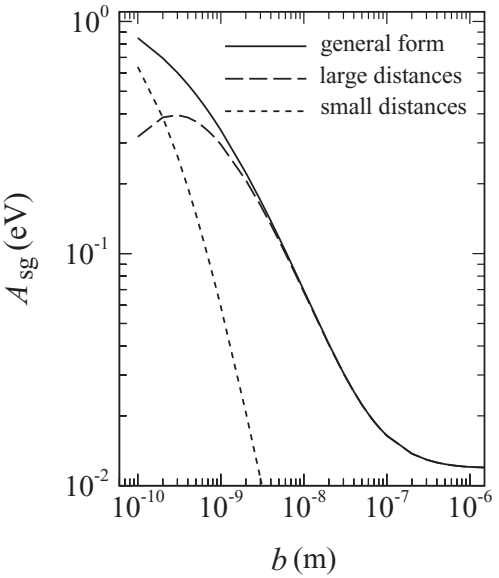

FIG. 10. Hamaker coefficient for a system of an undoped graphene layer apposed to a SiO_2 substrate as a function of the distance between them b. The top solid line shows the general form of the Hamaker coefficient as defined via Eq. (20), the dashed line shows the limiting large-distance form, Eq. (21), and the dotted line shows the limiting small-distance form, Eq. (22).

In Fig. 10, we again show the Hamaker coefficient as a function of the layer separation for a system comprising a SiO_2 substrate and an undoped graphene layer. We show the general form of the Hamaker coefficient from Eq. (20) (solid line) as well as the limiting forms at large [dashed line, Eq. (21)] and small [dotted line, Eq. (22)] separations. The large-distance limiting form obviously coincides with the general form at separations beyond 10 nm but again since the thickness of the graphene layer is only about 1 Å, the small-distance limiting form is expected to merge with the general form in subangstrom separations.

IV. VDW-CASIMIR INTERACTION IN A SYSTEM COMPOSED OF $N+1$ LAYERS OF GRAPHENE

In this section, we shall use the Lifshitz formalism in order to study the many-body vdW-Casimir interactions in a system composed of $N+1$ layers of graphene. The layers are separated from each other by N layers of vacuum and are bounded at the two ends by two semi-infinite dielectric slabs as depicted in Fig. 11. The thickness of each graphene layer is a, while the separation between two successive layers is b. We have labeled the left semi-infinite dielectric medium with L, the right one with R (which both will be assumed to be vacuum), the graphene layers with A, and the vacuum layers with B.

Following Ref. 32, one can calculate the vdW-Casimir part of the interaction free energy $F_N(a,b)$ in an explicit form for any finite N. Interestingly, it turns out that for very large values of N, the vdW-Casimir free energy can be written as a linear function of N so that the interaction free energy $F_N(a,b)$ becomes[32]

$$F_N(a,b) = N f_{gg}(a,b), \quad N \gg 1, \tag{23}$$

where $f_{gg}(a,b)$ can be interpreted as an effective pair interaction between two neighboring layers in the stack and is given by

$$f_{gg}(a,b) = k_B T \sum_{Q}{\sum_{n=0}^{\infty}}' \ln\left\{\frac{1-(\Delta^{(\mathrm{TM})})^2(e^{-2\kappa_A a}+e^{-2\kappa_B b})+e^{-2(\kappa_A a+\kappa_B b)}}{2[1-(\Delta^{(\mathrm{TM})})^2 e^{-2\kappa_A a}]} + \frac{1}{2}\sqrt{\frac{\mathcal{G}(a,b,\Delta^{(\mathrm{TM})})}{[1-(\Delta^{(\mathrm{TM})})^2\, e^{-2\kappa_A a}]^2}}\right\} + [(\mathrm{TM}) \to (\mathrm{TE})], \tag{24}$$

with $\mathcal{G}(a,b,\Delta^{(\mathrm{TM})})$ defined as

$$\begin{aligned}\mathcal{G}(a,b,\Delta^{(\mathrm{TM})}) = {} & [1-e^{-2(\kappa_A a+\kappa_B b)}]^2 - 2(\Delta^{(\mathrm{TM})})^2\{[e^{-2\kappa_A a} \\ & + e^{-2\kappa_B b}][1+e^{-2(\kappa_A a+\kappa_B b)}] - 4e^{-2(\kappa_A a+\kappa_B b)}\} \\ & + (\Delta^{(\mathrm{TM})})^4[e^{-2\kappa_A a}-e^{-2\kappa_B b}]^2.\end{aligned} \tag{25}$$

Here, $\Delta^{(\mathrm{TM})}$ is

$$\Delta^{(\mathrm{TM})} = \frac{\kappa_A \epsilon_B - \kappa_B \epsilon_A}{\kappa_A \epsilon_B + \kappa_B \epsilon_A}, \tag{26}$$

where κ_A and κ_B are

$$\kappa_{A,B}^2 = Q^2 + \xi_n^2 \epsilon_{A,B}(\iota\xi_n)/c^2. \tag{27}$$

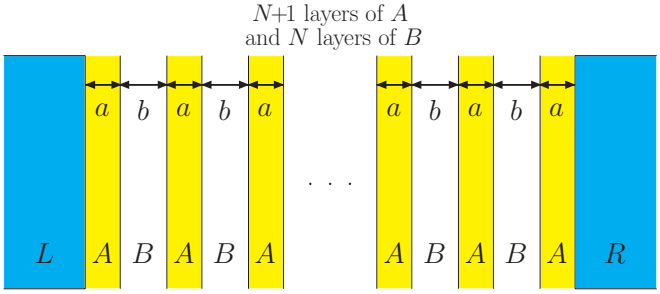

FIG. 11. (Color online) Schematic picture of the system composed of $N+1$ layers of graphene (A) with equal thicknesses a separated from each other by N layers of vacuum (B) with equal thicknesses of b. The two semi-infinite substrates in the left and right end of the system are labeled by L and R and will be assumed to be vacuum.

Again for the TE modes,

$$\Delta^{(\mathrm{TE})} = \frac{\kappa_A - \kappa_B}{\kappa_A + \kappa_B}. \tag{28}$$

For simplicity, we have dropped the explicit dependence on the Matsubara frequency in all the above expressions. We stress that $f_{gg}(a,b)$ is an effective pair interaction between two neighboring graphene layers in a multilayer geometry and is in general not equal to $F_{gg}(a,b)$ in Eq. (1), which is valid for two interacting layers in the absence of any other neighboring layers. The difference between these two interaction free energies thus encodes the nonpairwise additive effects in the interaction between two layers due to the presence of other vicinal layers.

A. $N+1$ undoped graphene layers

Let us first consider the case of $N+1$ undoped graphene layers. In this case, the vdW-Casimir interaction free energy per unit area and per number of layers, $|f_{gg}(b)|/S$ (black dot-dashed line), has been plotted in Fig. 12 as a function of the separation between the layers, b. The temperature of the system is chosen as 300 K, the thickness of the graphene layers is 1 Å and we have used the dielectric function given by Eq. (10) for each undoped graphene sheet.

The value of $|f_{gg}|/S$ at 1 nm is about 5.9×10^{14} eV/m^2, which is 5.9×10^2 eV when the surface area is equal to 10^{-12} m^2. At 10 nm, the value of $|f_{gg}|$ for the same surface area is about 0.01 eV and at 100 nm, is about 3.9×10^{-7} eV.

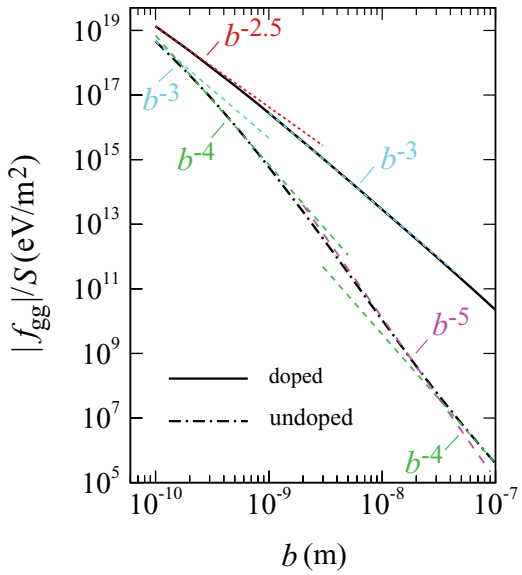

FIG. 12. (Color online) Magnitude of the interaction free energy per unit area and number of layers, $|f_{gg}|/S$, plotted as a function of the separation b between two successive undoped (bottom black dot-dashed line) and doped (top black solid line) graphene layers for a system composed of infinitely many layers of undoped/doped graphene as schematically depicted in Fig. 11. The temperature of the system is 300 K, the thickness of the graphene layers is fixed at 1 Å and we have chosen the dielectric function for the undoped case from Eq. (10) and for the doped case (with the doping electron density chosen as $\rho = 10^{16}$ m^{-2}), from Eq. (12). The functional form of the free energy for the undoped case is compared with scaling forms b^{-3}, b^{-4}, b^{-5}, and b^{-4} in various regimes of separation. For the doped case, the free energy is compared with the scaling forms $b^{-2.5}$ and b^{-3}.

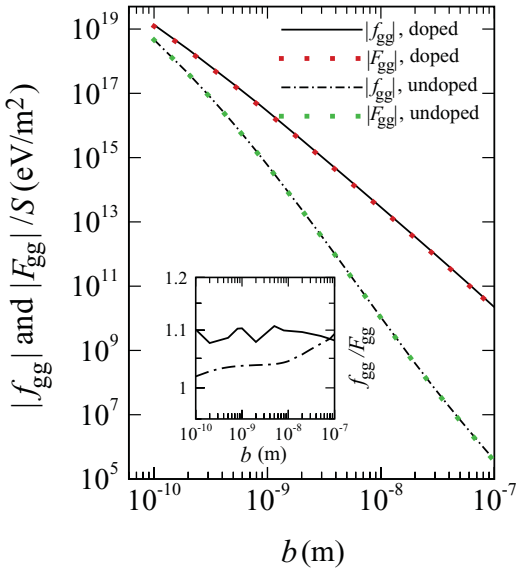

FIG. 13. (Color online) Magnitude of the interaction free energy per unit area and number of layers, $|f_{gg}|/S$, for the system composed of $N + 1$ layers of undoped (bottom black dot-dashed line) and doped (top black solid line) graphene is compared with the magnitude of the interaction free energy per unit area, $|F_{gg}|/S$, for the system composed of only two undoped (green dots) and doped (red dots) graphene layers as a function of the separation between the layers, b. The inset shows the ratio of these two quantities for both undoped (black dot-dashed line) and doped (black solid line) cases.

The scaling of $|f_{gg}(b)|/S$ for different values of the interlayer spacing b is shown in Fig. 12. It shows the scaling exponent $n = 3$ at vanishing separations, while at finite yet small separations, it is characterized by $n = 4$, continuously merging into an $n = 5$ form and finally attaining the $n = 4$ form. The rationalization of this sequence of scaling exponents is exactly the same as in the case of two isolated layers and will thus not be repeated here.

One can directly compare the reduced free energy $f_{gg}(b)$ with that of a system composed of only two undoped graphene layers of the same thickness a, $F_{gg}(b)$ (i.e., comparing the results in Fig. 2 with the corresponding results in Fig. 12). This is shown in Fig. 13 (black dot-dashed line and green dots), where by inspecting the ratio between these two interaction free energies one concludes that in the multilayer system the interaction free energy per layer is slightly more attractive than in the case of a two-layer system. This difference thus stems directly from the many-body effects, which in this case, augment the binding interaction in a graphitic stack.

B. $N + 1$ doped graphene layers

In Fig. 12, the magnitude of the vdW-Casimir interaction free energy for doped graphene layers per unit area and per number of layers, $|f_{gg}(b)|/S$, is plotted (black solid line) as a function of the separation between layers, b. The vdW-London dispersion transform of the dielectric function for each graphene sheet is chosen as in Eq. (12). We have fixed the density of electrons for all the graphene layers as $\rho = 10^{16}$ m^{-2}. The value of $|f_{gg}|/S$ at 1 nm is about 2.8×10^{16} eV/m^2, which is about 2.8×10^4 eV when the surface area is equal to 10^{-12} m^2. At 10 nm, the value of $|f_{gg}|$ is about 29 eV and at 100 nm, it is about 2.2×10^{-2} eV. The scaling exponents of the interaction free energy dependence for different regions of interlayer spacings are illustrated in Fig. 12.

The scaling exponent is $n = 2.5$ for vanishingly small separations, while at larger separations it tends toward the value $n = 3$. It is thus exactly the same as in the case of two isolated doped graphene sheets, see Fig. 3, except that in the multilayer geometry we have not shown the same range of separations as for two isolated layers.

The comparison of vdW-Casimir interaction free energies in the case of two isolated doped graphene sheets with the effective interaction between two graphene sheets in a multilayer system (i.e., comparing $|F_{gg}|$ in Fig. 3 with $|f_{gg}|$ in Fig. 12) is made in Fig. 13. As shown by the inset, the interaction free energy is again slightly more attractive within a multilayer. Comparing the results in the inset of Fig. 13, shows that in average, the many-body effects are stronger in the doped multilayer case than in the undoped case.

Note also that a direct comparison between the undoped and doped systems (see Fig. 12) shows that for all separations, the free energy magnitude for a doped multilayer (solid line) is more than that of the undoped one (dot-dashed line) and thus the interaction is more attractive in the former case. At separation 1 nm, the magnitude of the doped free energy is

TABLE I. A breakdown of the results on the scaling form of vdW-Casimir interactions in graphitic systems. The scaling exponent is defined in Eq. (11) and we have $\xi_T = \hbar v/k_B T \simeq 26$ nm and $\lambda_T = \hbar c/k_B T \simeq 300\xi_T$. We have not included our results on graphene sheet apposed to a dielectric substrate because they are not directly comparable to previous work.

Reference	System	T	$n(b)$	Comment
Dobson *et al.*[38]	two metallic sheets	$T = 0$	5/2	$b \ll \xi_T$
	two graphene sheets	$T = 0$	3	$b \ll \xi_T$
	graphene vs metallic sheet	$T = 0$	3	$b \gg \xi_T$
Gomez-Santos[39]	two graphene sheets	$T = 0$	3	$b \ll \xi_T$
	two graphene sheets	$T \neq 0$	3	$b \ll \xi_T$
	two graphene sheets	$T \neq 0$	2	$b \gg \xi_T$
	graphene vs dielectric sheet	$T \neq 0$	4	$b \ll \xi_T$
	graphene vs dielectric sheet	$T \neq 0$	5	$\xi_T < b < \lambda_T$
	graphene vs dielectric sheet	$T \neq 0$	4	$b \gg \lambda_T$
	graphene vs metallic sheet	$T \neq 0$	5/2	$b \ll \xi_T$
	graphene vs metallic sheet	$T \neq 0$	3	$\xi_T < b < \lambda_T$
	graphene vs metallic sheet	$T \neq 0$	2	$b \gg \lambda_T$
Bordag *et al.*[40]	graphene vs metallic sheet	$T = 0$	3	$b \ll \xi_T, m \neq 0$
	graphene vs metallic sheet	$T = 0$	4	$b \gg \xi_T, m \neq 0$
	graphene vs metallic sheet	$T = 0$	3	all b, $m = 0$
Fialkovsky *et al.*[41]	graphene vs metallic sheet	$T \neq 0$	3	$b \ll \xi_T$
	graphene vs metallic sheet	$T \neq 0$	2	$b \gg \lambda_T$
Sernelius *et al.*[25,33]	two metallic sheets	$T = 0$	5/2	nonretarded
	two graphene sheets	$T = 0$	3	nonretarded
present work	two undoped graphene sheets	$T \neq 0$	3	$b \ll \xi_T$
	two undoped graphene sheets	$T \neq 0$	4	$b \gg \xi_T$
	two doped graphene sheets	$T \neq 0$	5/2	$b \ll \xi_T$
	two doped graphene sheets	$T \neq 0$	2	$b \gg \xi_T$

about 47 times larger, while at the separation 10 nm, it is about 2650 larger than that of the undoped one.

V. CONCLUSION

In this work, we have studied the vdW-Casimir interaction between graphene sheets and between a graphene sheet and a substrate. We calculated the interaction free energy via the finite-temperature Lifshitz theory of vdW interactions that takes as an input the dielectric functions, or better their vdW-London transform, of isolated layers. Within this approach, it would be inconsistent to take into account any separation-dependent coupling between the dielectric response of the layers. This need possibly not be the case for some other approximate approaches to vdW interactions as in, e.g., the vdW augmented density functional theory (see the paper by Langreth *et al.*[22]).

By inserting the RPA dielectric function of a graphene layer into the finite-temperature Lifshitz theory, we are thus in a position to evaluate not only the pair interaction between two isolated graphene sheets, but also between a graphene sheet and a semi-infinite substrate of a different dielectric nature (SiO_2 in our case) as well as the effective interactions between two graphene sheets in an infinite stack of graphene layers. All these cases that have been analyzed and discussed above are relevant for many realistic geometries in nanoscale systems[12] and thus deserve to be studied in detail.

We note that in this work we focus on the direct temperature effects as given by the finite-temperature Lifshitz formula and the indirect temperature effects stemming from the temperature variation of the dielectric response of graphene are neglected. In general, this turns out to be a good approximation for a sufficiently high doping level at room temperature (as considered in the doped systems studied in this work) as finite-temperature effects in this case amount to a relatively small variation in the chemical potential and other electronic properties of graphene sheet (due to a relatively high Fermi temperature).[36] For an undoped system, the temperature effects are again negligible at sufficiently small separations as will be discussed below but can play a role in the behavior of the vdW-Casimir interaction at large separations. It should be also noted that the RPA approximation is itself strictly valid in the situations where electronic correlations are not too strong and thus, in particular at low doping levels, one may need to go beyond the standard RPA approach in order to describe correlation contributions on a more systematic level. This may be achieved by incorporating more sophisticated theoretical models for the dielectric response function which would be worth exploring further in the future.

Since several works[25,33,37–43] on vdW-Casimir interactions in graphitic systems are available, a proper comparison with those results seems to be in order (see Table I). Dobson *et al.* in their seminal work[38] focus on the zero-temperature cases of graphitic vdW-Casimir interactions. As shown by Gomez-

Santos,[39] the relevant thermal length for graphene below which the zero-temperature behavior should be expected is given by $\xi_T = \hbar v/k_B T$, which is about 26 nm and thus about 300 times smaller that the standard electromagnetic thermal length $\lambda_T = \hbar c/k_B T$. With this in mind for thin metallic sheets, Dobson *et al.* derive the scaling exponent $n = 5/2$. This compares favorably with doped graphene for small separations below ξ_T in our Fig. 3, since doped RPA graphene sheets behave similarly to ideal metals. For two graphene sheets, Dobson *et al.* derive $n = 3$ at $T = 0$, which should be compared with our undoped graphene case for small separations below ξ_T in our Fig. 2. Contrary to Dobson *et al.*, we do not analyze the case of a graphene layer apposed to an ideal metallic sheet where they again get the scaling exponent $n = 3$. However, this result agrees with the calculation of Bordag *et al.*[40] when the graphane's energy gap is set equal to zero.

Gomez-Santos in his work on thermal van der Waals interaction between graphene sheets[39] derives several results that are consistent with our calculations, where such a comparison makes sense. For two graphene sheets at zero temperature or finite temperature and small separations, $b \ll \xi_T$, Gomez-Santos gets $n = 3$ which is exactly the same as derived by Dobson *et al.*[38] and completely consistent with our Fig. 2 for two undoped graphene sheets. For finite temperature and large separations, $b \gg \xi_T$, we find $n = 4$ for undoped graphene, however, as noted above, finite-temperature effects are expected to play a role in this regime and the presence of thermally excited charge carriers (electrons and holes) when accounted for leads to an exponent similar to the doped case with $n = 2$ (see Fig. 3) as shown by Gomez-Santos[39] and also by Fialkovsky *et al.*[41] for a graphene layer apposed to a perfect conductor sheet. The results for graphene layer apposed to a dielectric sheet at finite temperatures are not directly comparable to our calculations since our model system comprises a graphene layer apposed to a dielectric half-space where we get scaling exponents $n = 3,4,3$, see Fig. 8, as opposed to $n = 4,5,4$ derived by Gomez-Santos. Here too the discrepancy is due to the difference in the models used. Gomez-Santos uses a thin dielectric sheet versus graphene layer, while we use a dielectric half-space, consistently explaining the higher scaling exponents in the former case. While we do not analyze specifically the case of a graphene layer apposed to an RPA electron metallic sheet, the scaling exponents $n = 5/2$ and $n = 2$ as derived by Gomez-Santos are again consistent with what we stated above. This case can be best compared with our Fig. 3 where we even see the exponent $n = 3$ at intermediate spacings.

Bordag *et al.*[40] analyze the case of a graphene layer with an explicit fermionic Lagrangian apposed to a perfect conductor sheet at zero temperature. The graphene sheet can even have a finite gap (mass) m, which is certainly not among the cases that we deal with. For $m = 0$, they recover the ideal Casimir metallic result at zero temperature but they do not find the $5/2$ scaling exponent neither for zero nor for finite temperature as seen in Refs. 38 and 39 and our work. The zero-temperature limit has been relaxed to include finite-temperature effects in a related work by Fialkovsky *et al.*,[41] based on the field theoretical methods as applied in the presence of spatial inhomogeneities.[42] The derived scaling exponent $n = 2$ is consistent with the finite-temperature Casimir interaction of ideal metals as well as with the asymptotic separation scaling form found in our Fig. 3, though we do not specifically address this case (graphene versus metallic sheet).

The results derived by Sernelius *et al.*[33] for the nonretarded interaction of two metallic sheets at zero temperature with $n = 5/2$ are again consistent with the scaling exponent derived for doped graphene layers at small separations, Fig. 3. His results for the nonretarded Casimir interaction between two free standing graphene sheets[25] at $T = 0$ showing the exponent $n = 3$ are on the other hand completely consistent with our undoped results as seen by inspection of Fig. 2 for $b \ll \xi_T$.

Last but not least, Barton in a series of papers[43] analyzed the Casimir effect of a hydrodynamic model of two infinitesimally thin apposed plasma sheets. It appears, however, that this model does not describe the electronic properties specific to graphene and does not give realistic predictions for the vdW-Casimir interactions.[40]

The conclusion of these detailed comparisons is therefore that where the comparison is appropriate, our results are consistent with previous work but they do extend to several pertinent cases not discussed before.

In summing up, for the three cases studied, we found the following salient features of the vdW-Casimir interaction dependence on the separation between the interacting bodies. (i) In a system composed of two graphene layers, we demonstrated that the vdW-Casimir interactions in the case of undoped graphene show scaling exponents identical to those displayed in the case of interacting thin dielectric layers. In the doped case, the scaling exponents are consistent with vdW-Casimir interactions between two thin metallic layers. (ii) In a system composed of a semi-infinite dielectric substrate and an undoped graphene layer, the vdW-Casimir interactions display scaling exponents expected for this asymmetric geometry. For a doped graphene layer, the exponents revert to the previous case of two doped graphene layers. (iii) In a multilayer system composed of many graphene sheets, the vdW-Casimir interaction scaling exponents are the same as in the case of two isolated layers but the interactions are stronger due to many-body effects as a consequence of the presence of other layers in the stack.

The main motivation for a detailed study of vdW-Casimir interaction between graphene sheets in graphite-like geometries is the fact that graphitic systems belong to closed-shell systems and thus display no covalent bonding, so that any bonding interaction is by necessity of a vdW-Casimir type. Its detailed characterization is thus particularly relevant for this quintessential nanoscale system.[12]

ACKNOWLEDGMENTS

We would like to thank B. Sernelius for providing us with a preprint of his work and to I. V. Fialkovsky for his valuable comments on a previous version of the manuscript. R.P. acknowledges support from ARRS through the program P1-0055 and the research project J1-0908. A.N. acknowledges support from the Royal Society, the Royal Academy of Engineering, and the British Academy. J.S. acknowledges generous support by J. Stefan Institute (Ljubljana) provided for a visit to the Institute and the Department of Physics of IASBS (Zanjan) for their hospitality.

*Corresponding author: a.naji@damtp.cam.ac.uk

[1] K. S. Novoselov, E. McCann, S. V. Morozov, V. I. Fal'ko, M. I. Katsnelson, U. Zeitler, D. Jiang, F. Schedin, and A. K. Geim, Nat. Phys. **2**, 177 (2006).

[2] A. K. Geim and K. S. Novoselov, Nat. Mater. **6**, 183 (2007).

[3] A. H. Castro Neto, F. Guinea, N. M. R. Peres, K. S. Novoselov, and A. K. Geim, Rev. Mod. Phys. **81**, 109 (2009).

[4] J.-H. Chen, C. Jang, S. Adam, M. S. Fuhrer, E. D. Williams, and M. Ishigami, Nat. Phys. **4**, 377 (2008).

[5] R. Saito, G. Dresselhaus, and M. S. Dresselhaus, *Physical Properties of Carbon Nanotubes*, 1st ed. (World Scientific, Singapore, 1998).

[6] R. F. Rajter, R. Podgornik, V. A. Parsegian, R. H. French, and W. Y. Ching, Phys. Rev. B **76**, 045417 (2007).

[7] A. Šiber, R. F. Rajter, R. H. French, W. Y. Ching, V. A. Parsegian, and R. Podgornik, Phys. Rev. B **80**, 165414 (2009).

[8] M. S. Dresselhaus, G. Dresselhaus, K. Sugihara, I. A. Spain, and H. A. Goldberg, *Graphite Fibers and Filaments*, Springer Series in Materials Science, 1st ed. (Springer-Verlag, New York, 1988).

[9] J.-C. Charlier, X. Gonze, and J.-P. Michenaud, Carbon **32**, 289 (1994).

[10] J.-C. Charlier, X. Gonze, and J.-P. Michenaud, Europhys. Lett. **28**, 403 (1994).

[11] A. N. Kolmogorov and V. H. Crespi, Phys. Rev. B **71**, 235415 (2005); Phys. Rev. Lett. **85**, 4727 (2000).

[12] R. H. French, V. A. Parsegian, R. Podgornik *et al*., Rev. Mod. Phys. **82**, 1887 (2010).

[13] A. Bostwick, T. Ohta, T. Seyller, K. Horn, and E. Rotenberg, Nat. Phys. **3**, 36 (2007); Z. Q. Li, E. A. Henriksen, Z. Jiang, Z. Hao, M. C. Martin, P. Kim, H. L. Stormer, and D. N. Basov, *ibid*. **4**, 532 (2008).

[14] X. Du, I. Skachko, F. Duerr, A. Luican, and E. Y. Anderia, Nature (London) **462**, 192 (2009); K. I. Bolotin, F. Ghahari, M. D. Shulman, H. L. Stormer, and P. Kim, *ibid*. **462**, 196 (2009).

[15] V. W. Brar *et al*., Phys. Rev. Lett. **104**, 036805 (2010); E. A. Henriksen, P. Cadden-Zimansky, Z. Jiang, Z. Q. Li, L.-C. Tung, M. E. Schwartz, M. Takita, Y.-J. Wang, P. Kim, and H. L. Stormer, *ibid*. **104**, 067404 (2010); A. Luican, G. Li, and E. Y. Andrei, Phys. Rev. B **83**, 041405(R) (2011); K. F. Mak, J. Shan, and T. F. Heinz, Phys. Rev. Lett. **106**, 046401 (2011); F. Ghahari, Y. Zhao, P. Cadden-Zimansky, K. Bolotin, and P. Kim, *ibid*. **106**, 046801 (2011).

[16] A. Bostwick, F. Speck, Th. Seyller, K. Horn, M. Polini, R. Asgari, A. H. MacDonald, and E. Rotenberg, Science **328**, 999 (2010).

[17] V. N. Kotov, B. Uchoa, V. M. Pereira, A. H. Castro Neto, and F. Guinea, e-print arXiv:1012.3484 (unpublished).

[18] Y. Barlas, T. Pereg-Barnea, M. Polini, R. Asgari, and A. H. MacDonald, Phys. Rev. Lett. **98**, 236601 (2007).

[19] M. Polini, R. Asgari, Y. Barlas, T. Pereg-Barnea, and A. H. MacDonald, Solid State Commun. **143**, 58 (2007); M. Polini, R. Asgari, G. Borghi, Y. Barlas, T. Pereg-Barnea, and A. H. MacDonald, Phys. Rev. B **77**, 081411(R) (2008); A. Qaiumzadeh and R. Asgari, *ibid*. **79**, 075414 (2009); New J. Phys. **11**, 095023 (2009); A. Qaiumzadeh, N. Arabchi, and R. Asgari, Solid State Commun. **147**, 172 (2008).

[20] E. H. Hwang and S. Das Sarma, Phys. Rev. B **75**, 205418 (2007); S. Das Sarma, E. H. Hwang, and W.-K. Tse, *ibid*. **75**, 121406(R) (2007); E. H. Hwang, B. Y.-K. Hu, and S. Das Sarma, *ibid*. **76**, 115434 (2007); Phys. Rev. Lett. **99**, 226801 (2007).

[21] M. Polini, A. Tomadin, R. Asgari, and A. H. MacDonald, Phys. Rev. B **78**, 115426 (2008).

[22] V. A. Parsegian, *Van der Waals Forces* (Cambridge University Press, Cambridge, 2005); M. Bordag, G. L. Klimchitskaya, U. Mohideen, and V. M. Mostepanenko, *Advances in the Casimir Effect* (Oxford University Press, New York, 2009); D. C. Langreth *et al*., J. Phys. Condens. Matter **21**, 084203 (2009); T. Emig, Int. J. Mod. Phys. A **25**, 2177 (2010); J. Schwinger, L. L. Deraad Jr., and K. A. Milton, Ann. Phys. (NY) **115**, 1 (1978); J. Sarabadani and M. F. Miri, Phys. Rev. A **84**, 032503 (2011).

[23] R. Podgornik, G. Cevc and B. Žekš, J. Chem. Phys. **87**, 5957 (1987).

[24] Je-Luen Li, J. Chun, N. S. Wingreen, R. Car I. A. Aksay, and D. A. Saville, Phys. Rev. B **71**, 235412 (2005).

[25] B. E. Sernelius, Europhys. Letts. **95**, 57003 (2011).

[26] H. Rydberg, M. Dion, N. Jacobson, E. Schröder, P. Hyldgaard, S. I. Simak, D. C. Langreth, and B. I. Lundqvist, Phys. Rev. Lett. **91**, 126402 (2003); J. Rohrer and P. Hyldgaard, Phys. Rev. B **83**, 165423 (2011).

[27] G. Veble and R. Podgornik, Phys. Rev. B **75**, 155102 (2007).

[28] R. Podgornik, P. L. Hansen, and V. A. Parsegian, J. Chem. Phys. **119**, 1070 (2003).

[29] F. Wooten, *Optical Properties of Solids* (Academic Press, New York, 1972).

[30] B. Wunsch, T. Stauber, F. Sols, and F. Guinea, New J. Phys. **8**, 318 (2006); X.-F. Wang and T. Chakraborty, Phys. Rev. B **75**, 041404 (2007); E. H. Hwang and S. Das Sarma, *ibid*. **75**, 205418 (2007).

[31] S. Gangadharaiah, A. M. Farid, and E. G. Mishchenko, Phys. Rev. Lett. **100**, 166802 (2008).

[32] R. Podgornik, R. H. French, and V. A. Parsegian, J. Chem. Phys. **124**, 044709 (2006).

[33] B. E. Sernelius and P. Björk, Phys. Rev. B **57**, 6592 (1998).

[34] J. Mahanty and B. W. Ninham, *Dispersion Forces* (Academic Press, New York, 1976).

[35] D. B. Hough and L. R. White, Adv. Colloid Interface Sci. **14**, 3 (1980).

[36] M. R. Ramezanali, M. M. Vazifeh, R. Asgari, M. Polini, and A. H. MacDonald, J. Phys. A: Math. Theor. **42**, 214015 (2009).

[37] S. A. Jafari *et al*. (unpublished).

[38] J. F. Dobson, A. White, and A. Rubio, Phys. Rev. Lett. **96**, 073201 (2006).

[39] G. Gómez-Santos, Phys. Rev. B **80**, 245424 (2009).

[40] M. Bordag, I. V. Fialkovsky, D. M. Gitman, and D. V. Vassilevich, Phys. Rev. B **80**, 245406 (2009).

[41] I. V. Fialkovsky, V. N. Marachevsky and D. V. Vassilevich, Phys. Rev. B **84**, 035446 (2011).

[42] I. V. Fialkovsky, V. N. Markov and Yu. M. Pis'mak, J. Phys. A: Math. Theor. **43**, 365401 (2010).

[43] G. Barton, J. Phys. A: Math. Gen. **38**, 2997 (2005); **38**, 3021 (2005).